Journal of Medicinal Chemistry

Article

pubs.acs.org/jmc

Comparative in Vitro Evaluation of N-Heterocyclic Carbene Gold(I) Complexes of the Benzimidazolylidene Type

Riccardo Rubbiani,[†] Suzan Can,[‡] Igor Kitanovic,[‡] Hamed Alborzinia,[‡] Maria Stefanopoulou,[§] Malte Kokoschka,[§] Susann Mönchgesang,[‡] William S. Sheldrick,[§] Stefan Wölfl,[‡] and Ingo Ott*[,†]

[†]Institute of Medicinal and Pharmaceutical Chemistry, Technische Universität Braunschweig, Beethovenstrasse 55, 38106 Braunschweig, Germany

[‡]Institut für Pharmazie und Molekulare Biotechnologie, Ruprecht-Karls-Universität Heidelberg, Im Neuenheimer Feld 364, 69120 Heidelberg, Germany

[§]Lehrstuhl für Analytische Chemie, Ruhr-Universität Bochum, 44780 Bochum, Germany

Supporting Information

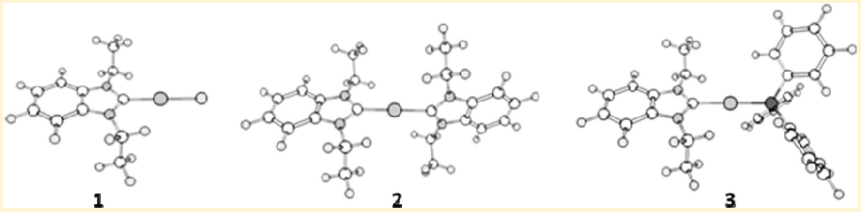

ABSTRACT: Gold(I) complexes with a 1,3-diethylbenzimidazol-2-ylidene N-heterocyclic carbene (NHC) ligand of the type NHC-Au-L (L = -Cl, -NHC, or -PPh_3) were comparatively evaluated as thioredoxin reductase (TrxR) inhibitors and antimitochondrial anticancer agents. Different effects were noted in various biochemical assays (e.g., inhibition of TrxR, cellular and mitochondrial uptake, or effects on mitochondrial membrane potential), and this was related to properties of the complexes such as bond dissociation energies and overall charge. Remarkable antiproliferative effects, a strong induction of apoptosis, and enhancement of reactive oxygen species (ROS) formation as well as other effects on tumor cell metabolism confirmed the promising potential of the complexes as novel anticancer chemotherapeutics.

INTRODUCTION

After the development of auranofin (see Figure 1) as an antirheumatic drug and the discovery of its antiproliferative properties, gold complexes started to play an increasing role in the search for new metal-based anticancer drugs. This was also motivated by findings that these metal compounds showed a different pharmacological behavior in comparison to the established platinum anticancer drugs. Over the last decades, several promising classes of gold-based drug candidates have been described.[1−4] Bischelating phosphines,[2,5] dithiocarbamates,[6,7] porphyrines,[8] or N-heterocyclic carbenes (NHC, see Figure 1 for examples)[9−11] are important examples of ligands used for coordination of the gold central atoms in new biologically active gold metallodrugs.

Different molecular targets related to distinct diseases have been described for gold complexes including the thioredoxin system,[12] phosphatases,[13,14] or very recently zinc finger proteins such as PARP-1.[15] The ubiquitous selenoenzyme thioredoxin reductase (TrxR) is considered as the one of the most critical targets for gold complexes, which have been reported to be potent and selective inhibitors of its catalytic activity.[12,16] TrxR is a NADPH-dependent flavoprotein responsible for cell homeostasis regulation and closely linked to many disease conditions including rheumatoid arthritis or cancer.[17] On the molecular level, a selenocysteine residue in the C-terminal active site of TrxR is considered as the ultimate target for gold species, and covalent binding with gold ions has been suggested as a mechanism.[18,19]

However, traditional gold complexes such as auranofin are readily metabolized by thiol-containing biomolecules, and the coordinated ligands are mostly lost before the target enzyme is reached.[20] The strong metabolization has so far hindered the rational design of gold metallodrugs and therefore the development of more stable gold complexes, and the fine tuning of their ligands is of particular interest. NHC ligands offer obvious advantages for this aim based on the high stability of their organometallic complexes and their fascinating biological potential, which has been documented in an increasing number of reports.[21−24]

Recently, we had reported a study on gold(I) NHC complexes of the benzimidazol-2-ylidene type that demonstrated promising biological features including the selective inhibition of TrxR and strong antiproliferative effects.[10] Compound **1**, which consists of a central gold(I) atom with a 1,3-diethylbenzimidazol-2-ylidene and a chlorido ligand, was studied exemplarily in more detail and showed a substantial potential as novel anticancer agent based on its ability to induce

Received: September 14, 2011
Published: October 31, 2011

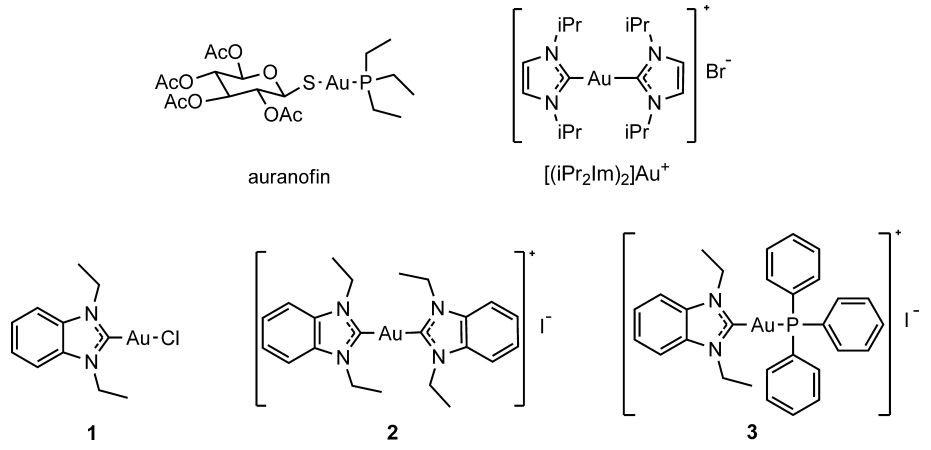

Figure 1. Examples of biologically active gold(I) complexes and target compounds of this study.

apoptosis and reactive oxygen species (ROS) formation, its activity against resistant types of cancer cells, as well as distinct effects on tumor cell metabolism. As metal NHC bonds are generally stable, the chloride of **1** could be expected to be the more labile ligand at the gold center of this complex. Replacement reactions involving the chloride should enable the compound to bind covalently to biological targets but also lead to inactivation and metabolization reactions. Complex **1** did not show reactions with glutathione in short exposure experiments in contrast to auranofin and chloro gold(I) phosphines, which are generally very reactive toward thiols.

To modify the pharmacodynamic properties of **1**, it was therefore of interest to introduce ligands, for which an even higher stability of the coordinative bonds could be expected. For this purpose, an additional NHC ligand and a phosphane were chosen, respectively. The coordination with these neutral ligands leads to the formation of cationic species (**2** and **3**), which also might display differing pharmacokinetic properties as a consequence of a modified drug biodistribution. The preparation and comparative biological studies of these complexes are described here.

COMPUTATIONAL CHEMISTRY

Before chemical synthesis, it was of interest to evaluate the stability of the coordinative bonds by theoretical methods. Bond dissociation energies (BDEs) and the geometry of the synthesized compounds have been investigated using density functional theory. During the past decade, density functional theory and Beckes three-parameter hybrid functional (B3LYP) in particular have evolved to be the workhorse in the field of molecular structure calculations. The low demand of density functional methods on computational resources is complemented by a high accuracy for many applications. BDEs of systems containing transition metals, obtained with B3LYP, were found to be of good quality.[25] For a set of cationic gold(I) complexes, results obtained with B3LYP were shown to be in agreement with post Hartree−Fock methods like CCSD(T) or second order Møller−Plesset theory.[26] Because of the nature of the resulting fragments, the employment of a diffuse basis set and the inclusion of solvent effects were vital. Solvent effects were introduced via the polarizable continuum model (PCM), and the basis set superposition error was reduced to less than 4% by using the diffuse basis set aug-cc-pVDZ and corrected for by the counterpoise correction.[27] The calculations confirmed the expected linear coordination geometry of the complexes **1**−**3** (see Figure S1 in the Supporting Information). The calculated BDEs around the gold central atoms are summarized in Table 1.

Table 1. BDEs between the Gold Center and Its Two Coordinated Ligands[a]

complex	BDE (kJ/mol)	
NHC−Au−L	NHC−Au	Au−L
1 (NHC−Au−Cl)	267.07	118.80
2 (NHC−Au−NHC)	225.39	225.39
3 (NHC−Au−PPh_3)	207.59	158.48

[a]NHC: 1,3-diethylbenzimidazol-2-ylidene; L: Cl (**1**), 1,3-diethylbenzimidazol-2-ylidene (**2**), or triphenylphosphine (**3**).

BDE values between the gold and the NHC ligand were all above 200 kJ/mol. Accordingly, for these gold carbon bonds, a high stability can be expected. Comparing the BDE values of the Au−Cl (**1**), Au−NHC (**2**), and Au−PPh_3 (**3**) bonds, the stability of the complexes increased in the order **1** < **3** < **2**. Overall, from these calculations, a difference in stability and activity between the complexes could be expected.

SYNTHESIS

The target complexes were obtained starting from 1,3-diethylbenzimidazolium iodide (Bim-I). The synthesis of **1** was previously described.[10] For the preparation of **2**, Bim-I was reacted with **1** and for the synthesis of **3** with triphenylphosphine gold(I) chloride in both cases in presence of a mild base (see Scheme 1). The products were isolated and purified by extraction or by column chromatography and characterized by ^{1}H NMR, ^{13}C NMR, ^{31}P NMR, mass spectrometry, and elemental analysis. Characteristic spectroscopic features of the complex formation included the disappearing of the proton signal at C^2 of Bimy-I in the ^{1}H NMR spectra and a strong shift of the C^2 carbon signal in ^{13}C NMR spectra. Thus, the C^2 carbon signal in ^{13}C NMR was downfield shifted from 141 (Bim-I) to 177 ppm in the case of **1** and to 190 ppm in the case of **2** and **3**. ^{31}P NMR measurements of **3** showed an upfield shift of approximately 1 ppm for the phosphorus signal when compared to triphenylphosphine gold(I) chloride.

dx.doi.org/10.1021/jm201220n | J. Med. Chem. 2011, 54, 8646–8657

Scheme 1. Synthesis Procedure of the Gold(I) Carbene Complexes

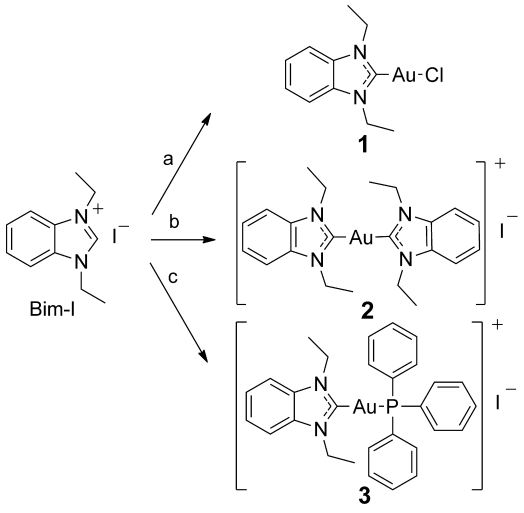

a) i) Ag_2O, rt, 5 h; ii) C_2H_6AuClS, rt, 10 h
b) K_2CO_3, rt, 12 h, chloro-(1,3-diethyl benzimidazol-2-ylidene) gold(I) chloride
c) K_2CO_3, rt, 8 h, $ClAuPPh_3$

BINDING OF GOLD(I) COMPLEXES TO SERUM ALBUMIN

The interaction with thiols is an important parameter in the biochemistry of gold-based drugs. It was shown that gold can be bound to the surface exposed Cys-34 of serum albumin, and a thiol shuttle model describing many thiol exchange processes has been proposed.[20,28] Complexes **1** and **2** were not reactive toward glutathione after short exposure (1 h) in a screening assay for thiol reactivity, whereas **3** showed some reactivity (see Figure S2 in the Supporting Information). Here, we studied the binding of **1**−**3** to bovine serum albumin by a precipitation method over a period of 24 h to evaluate the reactivity toward another biologically relevant thiol over an extended time frame under different conditions (see Figure 2). Auranofin was used as a reference. In good agreement with the published literature, auranofin showed a fast reaction (after 1 h binding of gold was almost complete) with 73% of the available gold bound to the protein after 6 h.[29] Complex **1** reacted somewhat slower, but overall protein binding was very similar to that of auranofin (66% after 6 h). Interestingly, **2** showed a comparably low protein binding, which was still below 20% after 6 h and did not exceed 50% after 24 h. For **3**, initial protein binding was 40−60% and increased to 87% over time. Whereas for auranofin and **1** stable values were reached within 1−2 h, binding continuously increased with the exposure time in the case of **2** and **3**. This indicates that the expected ligand exchange processes between the cysteine residue of albumin and the gold center are slowed down for the latter two complexes. Altogether, these results are in excellent agreement with the theoretical calculations above, which had indicated an order of reactivity **1** > **3** > **2**.

INTERACTION WITH A SELENOCYSTEINE-CONTAINING PEPTIDE

Advanced mass spectrometry can be used to determine the covalent binding abilities of new metallodrugs to proteins and peptide fragments.[18,30,31] To resemble the interaction with selenocysteine-containing enzymes closely, we used a seleno-cysteine-containing peptide (Ala-Gly-Sec-Val-Gly-Ala-Gly-Leu-Ile-Lys, AGUVGAGLIK). Initial studies using triphenylphos-phine gold(I) chloride as a positive reference confirmed covalent binding of gold to the selenocysteine residue (data not shown). Exposure of the seleno-peptide to complexes **1**−**3** followed by MS ionization led in all cases to molecular ions at

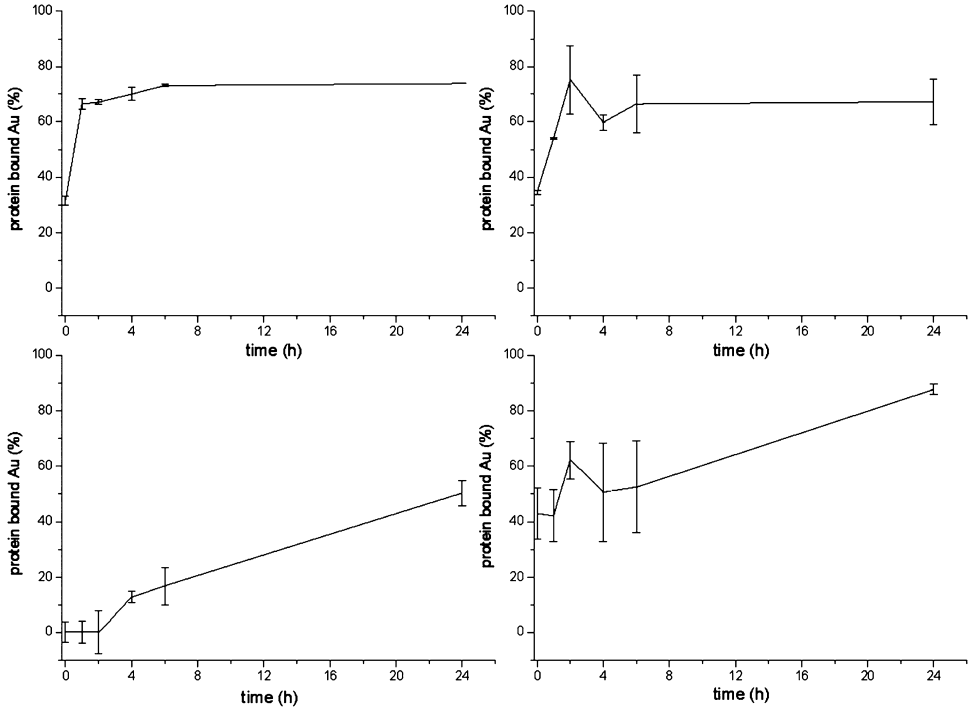

Figure 2. Binding of gold(I) complexes to bovine serum albumin: auranofin (top left), **1** (top right), **2** (bottom left), and **3** (bottom right); results are expressed as means (±errors) of repeated experiments.

dx.doi.org/10.1021/jm201220n | J. Med. Chem. 2011, 54, 8646–8657

m/z 1306 and 1134 corresponding to a gold diethylbenzimidazolylidene fragment or a single gold ion being respectively attached to the peptide. MS/MS analysis of these molecular ions contained appropriate modified and unmodified series of b^+ and y^+ fragment ions that confirmed the selenocysteine residue as the major binding site (see Figure 3). This indicated

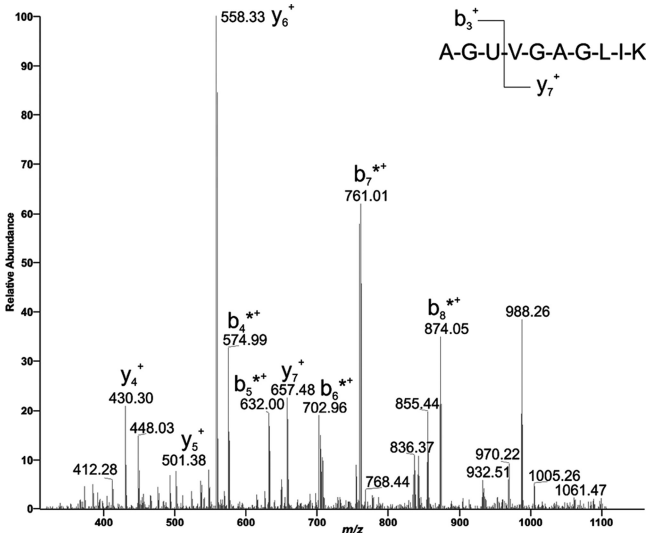

Figure 3. MS/MS spectrum of the molecular ion [peptide + Au]$^+$ at m/z 1134 formed by ionization of a 5:1 mixture of complex **1** with the selenopeptide H-AGUVGAGLIK-OH after a 48 h incubation at 37 °C. One asterisk (*) represents a gold atom. MS/MS spectra for **2** and **3** are given in Figure S3 in the Supporting Information.

that covalent binding to selenium can indeed be expected to be the dominating mechanism of molecular interaction for the herein presented gold complexes.

INHIBITION OF THE MAMMALIAN DISULFIDE REDUCTASES TRXR, GLUTATHIONE REDUCTASE (GR), AND GLUTATHIONE PEROXIDASE (GPX)

Having established the reactivity of **1**−**3** toward albumin- and selenocysteine-containing peptides, it was of interest to study the inhibitory properties toward the target enzyme TrxR. The structurally closely related GR as well as GPx as another selenoenzyme were investigated to obtain information on the selectivity of enzyme inhibition (see Table 2). The TrxR activity was efficiently inhibited by all three compounds with the order of activity **1** > **3** > **2**, which agrees well with the reactivities noted in the above-described studies. Whereas **1** and **3** exhibited EC_{50} values against TrxR well below 1 μM, the activity of **2** dropped to 4.89 μM. Concerning the inhibition of GR, the order of activity was changed to **3** > **1** > **2**. However, EC_{50} values were substantially higher in all cases, demonstrating that TrxR could be addressed with certain selectivity. For **2**, an EC_{50} value with GR could not be determined up to the highest concentration used (100 μM). The GPx activity was only inhibited by **1** with an EC_{50} approximately 30-fold higher than that observed with TrxR, which demonstrates that the compounds are not unspecific selenoenzyme inhibitors. The gold free Bim-I was inactive against all three enzymes, confirming that the gold center is required to obtain potent inhibitors.

EFFECTS ON TUMOR CELL GROWTH

The triggering of antiproliferative effects by the target coordination compounds was investigated in MCF-7 human breast adenocarcinoma and HT-29 colon adenocarcinoma cells (see Table 3). HEK-293 human embryonic kidney cells were used as a reference to determine a possible bioselectivity. As previously described, the gold free ligand Bim-I was not showing any influence on tumor cell proliferation. Relevant activities with IC_{50} values in the micromolar and submicromolar range could be observed for **1**−**3** in both cancer cell lines. Interestingly, the substitution of the chloride leaving group in **1** with the NHC and phosphine ligands in **2** and **3** led to an approximately 5-fold increase in antiproliferative potency in MCF-7 cells as well as an approximately 15-fold increase in HT-29 cells. Concerning bioselectivity, only compound **2** showed some preference for tumor cells over nontumorigenic cells HEK-293.

Table 3. IC_{50} Values for Antiproliferative Effects in MCF-7, HT-29, and HEK-293 Cells; Results Are Expressed as Means (±Errors) of Repeated Experiments

	IC_{50} (μM)		
	MCF-7	HT-29	HEK-293
Bim-I	>100[a]	>100[a]	>100[a]
1	4.57 ± 0.03[a]	6.41 ± 1.97[a]	10.3 ± 1.10[a]
2	0.81 ± 0.13	0.44 ± 0.13	3.13 ± 0.54
3	0.89 ± 0.40	0.40 ± 0.18	0.41 ± 0.18

[a]Values are from ref 10. Examples of dose−response curves are provided in Figure S4 in the Supporting Information.

To monitor direct effects on cell morphology, video microscopic imaging of MCF-7 cells exposed **1**−**3** was performed over a period of 14 h. Applied concentrations were chosen, taking into account the outcome of the proliferation experiments, and were 1.0 μM for **2** and **3** and 5.0 μM for the less active **1**. Whereas for **1** just a sporadic loss of single cells was observed, which was more evident at the end of the experiment, for **2** and **3**, a faster and stronger reduction of the cell layer could be noted. This was accompanied by an alteration of cell morphology and cell swelling starting after approximately 8−10 h of incubation (see Figure 4 and the video files in the Supporting Information). Overall, these data indicated that for **1** cell growth inhibition is mostly related to an

Table 2. Inhibition of TrxR, GR, and GPx; Results Are Expressed as Means (±Errors) of Repeated Experiments

	EC_{50} TrxR (μM)	EC_{50} GR (μM)	EC_{50} GPx (μM)	selectivity GR/TrxR	selectivity GPx/TrxR
Bim-I	>100[a]	>100[a]	>100		
1	0.36 ± 0.04[a]	8.70 ± 0.01[a]	10.8 ± 0.95	24-fold	30-fold
2	4.89 ± 1.15	>100	>100	>20-fold	>20-fold
3	0.66 ± 0.02	2.60 ± 0.55	>100	3.9-fold	>150-fold

[a]Values are from ref 10.

dx.doi.org/10.1021/jm201220n | J. Med. Chem. 2011, 54, 8646−8657

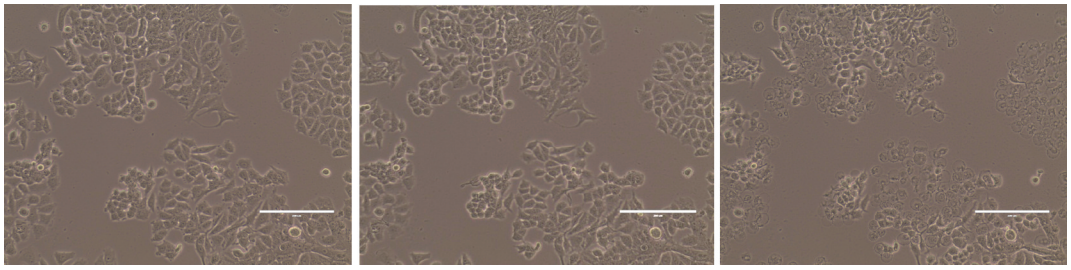

Figure 4. Influence of 1.0 μM **2** on MCF-7 cells after an incubation time of 0 (left), 2 (center), and 8 h (right). The scale bar represents a distance of 200 μm. Similar effects as with **2** were observed with **3**.

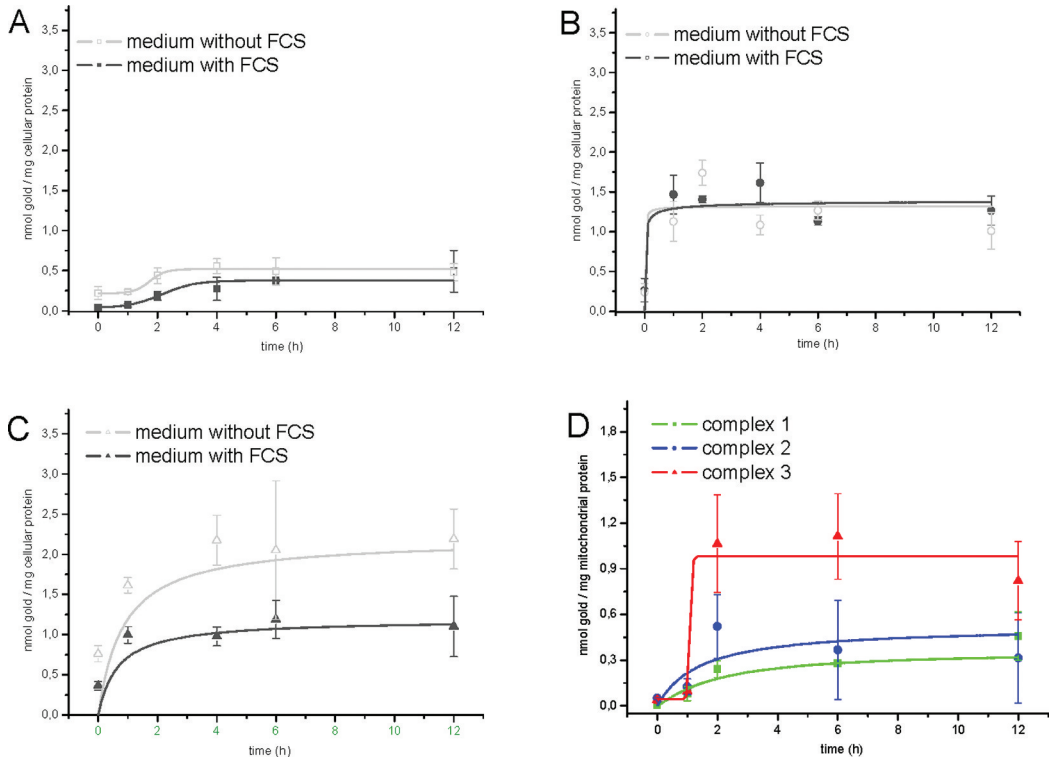

Figure 5. Time-dependent gold uptake into MCF-7 cells exposed to 3 μM **1** (A), **2** (B), and **3** (C). (D) Mitochondrial uptake of 3.0 μM of the gold complexes **1**–**3**; FCS, fetal calf serum. Results are expressed as means (±errors) of repeated experiments.

inhibition of cell proliferation (cytostatic effect), whereas for the cationic species **2** and **3** also direct cytotoxic effects play a major role.

CELLULAR UPTAKE AND BIODISTRIBUTION INTO MITOCHONDRIA

Complex **1** is a rather lipophilic neutral compound that could easily penetrate through the plasma membrane by simple passive diffusion. In contrast, **2** and **3** are positively charged but also lipophilic species. For these, properties similar to those observed with delocalized lipophilic cations could be expected. This includes permeation through the cell membrane and strong accumulation in the mitochondria.[32] Consequently, we evaluated the cellular uptake as well as the biodistribution of the complexes **1**–**3** by atomic absorption spectroscopy. According to results from the albumin binding studies, the cellular uptake experiments were done in a comparative manner using serum supplemented and serum-free cell culture media (see Figure 5A–C).

In the experiments with serum-free culture media, gold uptake increased in the order **1** < **2** ≤ **3**, and the complexes reached stable cellular levels within the first 2–4 h of incubation. The presence of the serum did not notably affect the cellular uptake of **2**, which had shown a rather low affinity for binding albumin (see above). For **1** and **3**, which had shown higher protein binding, cellular gold levels in the presence of serum were decreased, indicating that protein binding negatively influenced the uptake of these two gold complexes. This effect was more marked for **3**.

Next, the uptake of **1**–**3** into mitochondria isolated from MCF-7 cells exposed to a 3 μM concentration of the complexes was evaluated (see Figure 5D). To avoid effects of albumin or other serum components, the experiments were done using serum-free cell culture media. The gold levels increased in the order **1** ≤ **2** ≪ **3**, and similar to the overall uptake studies, stable levels were obtained within the first four hours of exposure. The result that stands out is the exceptionally high mitochondrial uptake of **3**. In part, this can be related to its high cellular uptake and its lipophilic cationic character. However, on the basis of the results above, a similar strong uptake of **2** could have been expected. During the isolation procedure of the mitochondria, additional cytosolic fractions were obtained

dx.doi.org/10.1021/jm201220n | J. Med. Chem. 2011, 54, 8646–8657

and were also investigated for their gold content. The gold levels in these samples were comparably low (see Figure S5 in the Supporting Information), implicating that the uptake into the mitochondria may be a major pathway for biodistribution of the complexes.

EFFECTS ON ISOLATED MITOCHONDRIA

In good agreement with the antimitochondrial effects described for many gold complexes and its inhibitory effects on TrxR activity, **1** had demonstrated strong effects on the respiration of isolated mice liver mitochondria in our previous study.[10] In addition to that, **2** and **3** represent cationic gold species, which can be accumulated in mitochondria and affect their biochemistry.[5,9] Therefore, it was of high interest to investigate the effects of the novel complexes on mitochondrial respiratory functions. For this purpose, an assay measuring the oxygen consumption of isolated, functionally active, mitochondria was applied.[10] As expected, strong effects were observed in a concentration-dependent manner with both **2** and **3**, which lowered respiration in concentrations as low as 0.1 μM and completely blocked respiration at 1.0 μM. Thus, they surpassed the activity of **1** in this assay, which had been active in concentrations of 5.0 μM and higher. The overall order of activity was **1** < **3** < **2** (see Figure 6).

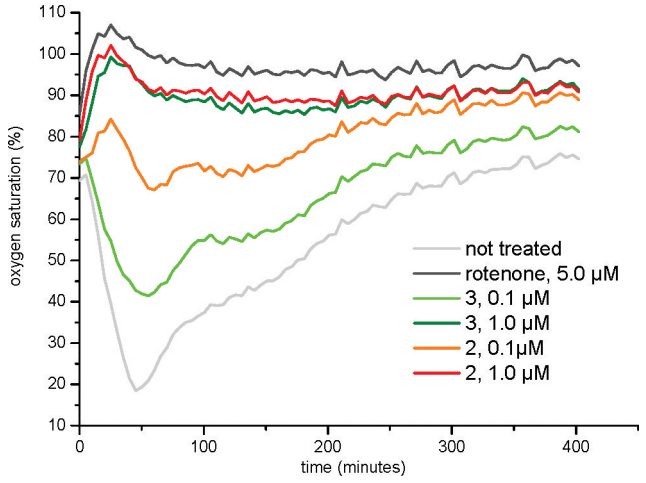

Figure 6. Respiration of freshly isolated mouse liver mitochondria. Mitochondrial activity leads to a decrease in oxygen saturation, which increases again over time (not treated). Inhibition of mitochondrial activity blocks oxygen consumption, resulting in continuous high oxygen concentration. Rotenone, an inhibitor of respiratory chain complex I and carbonyl cyanide 3-chlorophenylhydrazone (CCCP leads to decoupling of respiration and to an increased oxygen consumption; data not shown), served as negative and positive controls, respectively.

The regulation of Ca^{2+} signaling and its release play a central role in the homeostasis of mitochondria and cells. The mitochondrial membrane potential (MMP) produced during oxidative phosphorylation largely contributes to its control and reuptake. A modification in the electrical properties of the membrane can provoke an alteration in mitochondrial membrane permeability, the formation of the mitochondrial apoptosis-induced channel, and trigger programmed cell death.[33,34]

Complexes **1**–**3** influenced the MMP in different ways (see Figure 7). Complexes **1** and **3** induced after short incubation a

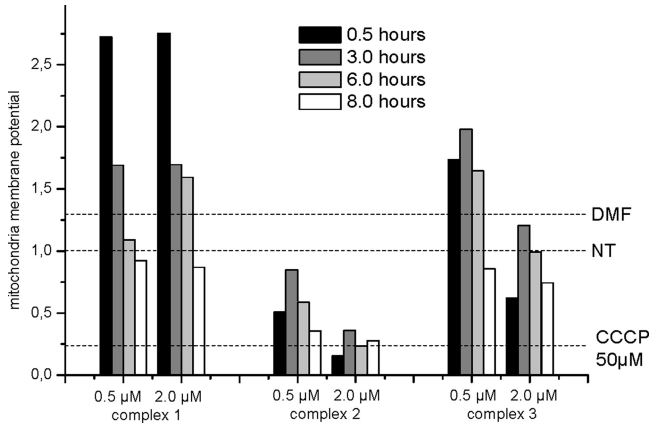

Figure 7. Influence on MMP normalized to an untreated control; NT, not treated. CCCP was used as a positive control.

strong hyperpolarization and after 8 h a small depolarization that can lead to Ca^{2+} release and possible activation of apoptotic processes. The effect was more pronounced for **1**. In contrast to that, complex **2**, the most active derivative, triggered an immediate and strong depolarization, which is in accordance with its exceptionally strong effects on mitochondrial respiration (see above).

A strong onset of mitochondria homeostasis can also induce the release of cytochrome *c* as another possible apoptosis intermediate.[35] Accordingly, released cytochrome *c* levels were studied by Western blot experiments with mitochondria exposed to effective concentrations of **1**–**3** (see Figure S6 in the Supporting Information). However, the results do not indicate a contribution of the mentioned pathway, as no detectable levels of cytochrome *c* were present in the supernatants of the mitochondrial suspensions (with the exception of a marginally positive signal with 10 μM of **1**).

EFFECTS ON ROS FORMATION, APOPTOSIS INDUCTION, AND TUMOR CELL METABOLISM

The strong cellular uptake and the interaction with TrxR and with mitochondrial biochemistry were reflected in strong antiproliferative effects of **1**–**3** and are expected to trigger also more specific effects on tumor cell metabolism. Accordingly, we investigated the effects of **1**–**3** in several relevant assays. Initially, the induction of ROS was studied. In good agreement with the results of the proliferation assay, increasing concentrations of **1**–**3** strongly enhanced cellular ROS levels (see Figure 8) in a concentration-dependent manner. This pattern also correlates well with the above observation that the gold compounds affected the activities of the redox enzymes TrxR and GR.

Experiments on the apoptosis and/or necrosis inducing activity of **1**–**3** were done by using the Annexin/PI assay (see Figure 9A). As previously reported, **1** influenced vital cells accompanied by a significant relative increase of necrotic cells and a low percentage of apoptotic cells in concentrations of 2.5 μM and higher.[10] Complex **2** induced apoptosis in concentrations above 1.0 μM with cells in the early and late stages of the apoptotic process. Similarly, **3** induced apoptosis in concentrations above 0.5 μM, however, leading to drastically more pronounced effects with most of the cells reaching the late apoptotic stages.

The influence of **1**–**3** on cellular metabolism was monitored in real time by the use of a biosensor chip analysis system

dx.doi.org/10.1021/jm201220n | J. Med. Chem. 2011, 54, 8646–8657

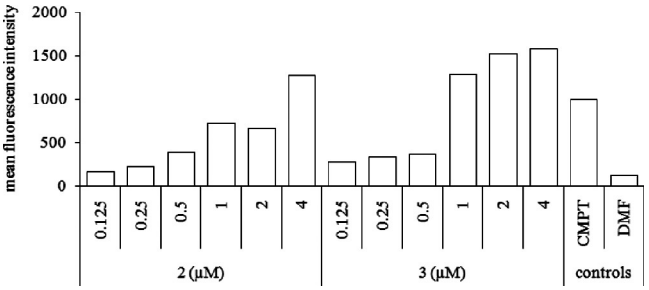

Figure 8. Induction of ROS formation by **2** and **3** in Jurkat cells after 48 h of exposure; CMPT and DMF were used as positive and negative controls, respectively. Similar results were observed after 24 h of exposure (see Figure S7 in the Supporting Information). Data concerning complex **1** were reported in ref 10.

(Bionas 2500), which allows the evaluation of the impedance of the cell layer, the respiration rate (oxygen consumption), and the acidification rate (glycolysis) of living cells over an extended time span (see Figure 9B–D).[36] Compound **1** had shown an immediate decrease of cell respiration and increased acidification rate followed by a strong decrease of cell impedance after extended exposure.[10] Analogously with **2** and **3**, the standard respiration rate was immediately lowered, and the acidification rate was decreased after an initial increase that suggests a glycolysis enhancement to compensate for the reduced respiration. Cell impedance started to decrease after approximately 10 h of exposure to the gold complexes **2** and **3**, which is indicative of morphological changes of the cells, changes in cell membrane properties, cell–cell contacts, and cellular adhesion. Acquired results complied with the morphological changes of cells after extended incubation observed during the microscopic live-cell imaging. Cells showed no recovery when **2** and **3** were removed from the medium after 13 h of treatment, indicating the effects on cell metabolism were irreversible.

CONCLUSIONS

NHC gold(I) complexes of the 1,3-benzimidazol-2-ylidene type with different ligands (−Cl, −NHC, and $-PPh_3$) were prepared, structurally characterized, and biologically investigated in a comparative manner. Initial DFT calculations revealed differences in BDEs, which indicated an order of stability **1** < **3** < **2**. The different BDE of the complexes led to different reactivities concerning binding to albumin and inhibition of the target enzyme TrxR. The chlorido derivative **1** was a strong and selective inhibitor of TrxR and showed an intensive binding to albumin similar to auranofin. The cationic complex **2** with two NHC ligands exhibited the lowest inhibition of TrxR and had the lowest binding capacity to albumin. Finally, the triphenylphosphine derivative **3** led to a strong inhibition of TrxR and also to an increased protein binding. Generally, TrxR was inhibited preferentially over structurally related enzymes (GR and GPx), and MS studies with a selencysteine-containing model peptide indicated that covalent interactions with selenium are highly relevant for the molecular mechanism of drug action.

The cationic charge of **2** and **3** and the rather large lipophilic character of their ligands may attribute the features known for delocalized lipophilic cations (DLC). DLCs can penetrate the hydrophobic barriers of the cellular membranes and accumulate in mitochondria in response to the electric gradient between

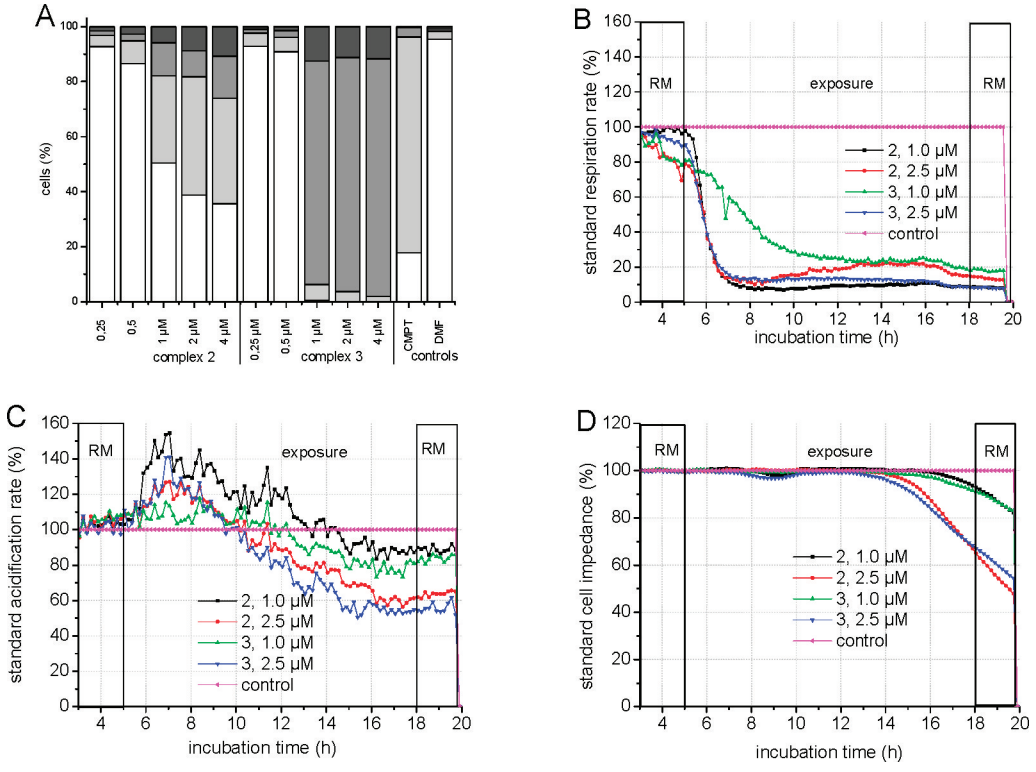

Figure 9. (A) Annexin/PI assay with Jurkat cells exposed to **2** and **3** for 48 h (black, necrotic cells; dark gray, late apoptotic; light gray, early apoptotic; and white, viable; CMPT was used as a positive control). (B–D) Concentration-dependent effects of **2** and **3** on the respiration rate (B), cellular acidification (C), and impedance (D) of MCF-7 cells. Data with **1** have been reported in ref 10; RM, "running medium" (without compound).

dx.doi.org/10.1021/jm201220n | J. Med. Chem. 2011, 54, 8646–8657

the membranes' inner and outer layers. It has also been reported that there is a difference of around 60 mV between the MMPs of cancerous and healthy cells that will induce a selective accumulation in tumor cell mitochondria.[33,37] Concerning the biochemistry of cationic gold(I) complexes, Berners−Price et al. have clearly demonstrated in a number of reports that "DLC effects" have a very high relevance.[9,38,39] In fact, cellular uptake studies with **1**−**3** showed that the gold uptake for the cationic species **2** and **3** was approximately 3-fold higher than for the neutral **1**, and gold levels of mitochondria isolated from cells exposed to **1**−**3** increased in the order **1** ≤ **2** ≪ **3**. The increased cellular and mitochondrial uptake of **2** and **3** was translated into enhanced antiproliferative effects and apoptosis induction in cancer cells as well as an induction of ROS formation.

The complexes induced apoptosis in a cytochrome *c* release independent manner. In particular, for **2**, the alteration of the normal MMP, induction of membrane permeability, and release of pro-apoptotic factors suggest another mitochondria-mediated apoptosis pathway.[33,37] Strong antimitochondrial effects could also be noted concerning mitochondrial respiration and were again most marked for **2**. Phase contrast video imaging indicated a deep change of the cell morphology after an incubation time of almost 10 h for **2** and **3**, which was also confirmed by experiments on cell impedance. Early effects of the gold complexes were noted on cell respiration.

Summarizing the results obtained with **1**−**3**, it can be concluded that their pharmacodynamic pattern is mainly the consequence of several pathways related to the inhibition of TrxR but also to distinct effects against mitochondrial biochemistry not necessarily related to TrxR inhibition. The introduction of a positive charge turned out to be a key feature to increase the cellular uptake, induce mitochondrial accumulation, and improve general cytotoxic properties. This could be related to effects commonly known for DLCs. The modulation of the stability of the coordinative bonds of the complexes affected the reactivity toward the target enzyme TrxR and general reactivity. Cationic complexes with a phosphine and NHC ligand such as **3** might provide a useful compromise between good inhibitory effects against TrxR and strong antiproliferative/antimitochondrial properties.

EXPERIMENTAL SECTION

General. All reagents and the solvents were used as received from Sigma Aldrich, Acros Organics, or other commercial suppliers. ^{1}H NMR and ^{13}C NMR were recorded on a Bruker DRX-400 AS, and mass spectra were recorded on a Finnigan MAT 4515 and an LTQ XL instrument (Thermo Electron Corp.). MCF-7 breast adenocarcinoma, HT-29 colon carcinoma, and HEK-293 human embryonic kidney healthy cells were maintained in DMEM High Glucose (PAA laboratories GmbH), supplemented with 50 mg/L gentamycin (USBiological) and 10% (v/v) fetal calf serum (FCS, Biochrom AG) prior to use. Jurkat cells were cultured in RPMI 1640 supplemented with 10% (v/v) FCS. A purity of ≥95% of all synthesized compounds was confirmed by elemental analyses (Flash EA112, Thermo Quest Italia). For all compounds undergoing biological evaluation, the experimental values differed less than 0.5% from the calculated ones.

Synthesis. 1,3-Diethylbenzimidazolium iodide and complex **1** were obtained following an established procedure.[10] Complexes **2** and **3** were obtained by similar procedures as described for related compounds.[9,40]

[Di-(1,3-diethylbenzylimidazol-2-ylidene)]gold(I) Iodide (2). Diethylbenzimidazolium iodide (0.151 g, 0.5 mmol) was stirred with complex **1** (0.203 g, 0.5 mmol) and K_2CO_3 (0.069 g, 0.5 mmol) for 12 h in 10 mL of dichloromethane/methanol (1/1). The formed product was isolated by column chromatography (eluent: dichloromethane/methanol 97.5/2.5). Yield: 0.202 g (0.3 mmol, 43%) white powder. ^{1}H NMR ($CDCl_3$): (ppm) 1.69 (t, 12H, ^{3}J = 9.7 Hz, CH_3), 4.72 (q, 8H, ^{3}J = 9.7 Hz, CH_2), 7.46 (dd, 4H, ^{4}J = 4.4 Hz, ^{3}J = 8.2 Hz, ArH_4), 7.58 (dd, 2H, ^{4}J = 4.4 Hz, ^{3}J = 8.2 Hz, ArH_5). ^{13}C NMR ($CDCl_3$): (ppm) 16.0 (CH_3), 44.2 (CH_2), 111.6 (ArC_8), 124.6 (ArC_4), 133.1 (ArC_5), 190.3 (NHC). MS (EI): 498 (M^+ − NHC). MS (ESI): 672 (M^+), 545 (M^+ − I). Elemental analysis for $C_{22}H_{28}AuN_4I$ (% calcd/found): C (39.18/39.08), H (4.48/4.22), N (8.31/8.06).

[Triphenylphosphine-(1,3-diethylbenzylimidazol-2-ylidene)]gold(I) Iodide (3). Complex **3** was synthesized starting from the 1,3-diethylbenzimidazolium iodide (0.151 g, 0.5 mmol) with triphenylphosphine gold chloride (0.247 g, 0.5 mmol) in the presence of a K_2CO_3 (0.069 g, 0.5 mmol), under vigorous stirring for 8 h in dichloromethane. The substance was purified through liquid/liquid extraction with dichloromethane/water, and the organic solvent was afterward evaporated to give the pure product. Yield: 0.228 g (0.3 mmol, 58%) white powder. ^{1}H NMR ($CDCl_3$): (ppm) 1.68 (t, 6H, ^{3}J = 9.7 Hz, CH_3), 4.71 (q, 4H, ^{3}J = 9.7 Hz, CH_2), 7.52 (m, 19H, ArH). ^{13}C NMR ($CDCl_3$): (ppm) 16.0 (CH_3), 44.2 (CH_2), 111.6 (ArC_8), 124.7 (ArC_4), 128.8 ($PArC_1$), 128.9 ($PArC_2$), 130.6 (ArC_5), 134.0 ($PArC_3$), 134.1 ($PArC_4$), 190.2 (NHC). ^{31}P NMR: (ppm) 32.5. MS (EI): 586 (M^+ − NHC), 498 (M^+ − PPh_3). MS (FAB): 760 (M^+). Elemental analysis for $C_{29}H_{29}AuN_2PI$ (% calcd/found): C (45.75/46.24), H (3.97/3.83), N (3.68/3.56).

Computational Chemistry. All calculations were performed using Gaussian 03 (Rev. E.01).[41] Density functional theory (B3LYP) has been employed for all geometry and energy calculations. Geometries and zero point corrections were calculated using the Stuttgart RSC 1997 ECP (SDD) basis set on Au and the 6-31G(d) basis set on all other atoms. An ultrafine grid had to be employed for PPh_3-containing molecules to reach convergence. For the calculation of energies, the diffuse basis sets aug-cc-pVDZ-PP on Au and aug-cc-pVDZ on all other atoms were used. The basis sets Stuttgart RSC 1997 ECP, aug-cc-pVDZ, and aug-cc-pVDZ-PP have been obtained via the EMSL Web site Basis Set Exchange.[42,43] The final energy values were corrected for the basis set superposition error using the counterpoise method according to Boys and Bernardi.[27] To account for solvent effects, the polarizable continuum model (IEF-PCM)[44−46] was employed with ε = 78.39 for water. All illustrations of molecular structures obtained from ab initio calculations were prepared using Chemcraft.

Binding to Albumin. The gold(I) complexes were prepared as stock solutions in dimethylformamide to achieve a final concentration of 3.0 mM. A 440 mg amount of bovine serum albumin (BSA, Sigma Aldrich) was dissolved in 11.0 mL of cell culture medium. Eleven microliters of the gold complex stock solutions was added to the BSA-containing medium and incubated at 37 °C in the dark under gentle shaking. After 0, 1, 2, 4, 6, and 24 h, a 250 μL aliquot thereof was taken, treated with 500 μL of cold (−20 °C) ethanol, and stored at −20 °C for 2 h to allow precipitation of the protein fraction. Afterward, the solution was centrifuged at 400*g* for 5 min at 4 °C, 400 μL of the supernatant was taken, treated with 40 μL of 13% HNO_3, and the gold content was measured by AAS (see below). The percentage of gold bound to albumin was calculated thereof. Results are given as the means and errors of repeated two independent experiments.

Atomic Absorption Spectroscopy. Gold contents were measured with a graphite furnace high resolution atomic absorption spectrometer (contra AA 700, Analytik Jena AG) at 242.795 nm according to a recently described method with minor modifications in the graphite furnace temperature program (see Table S1 in the Supporting Information).[47] Matrix-matched calibration with gold standard solutions (Fluka) was used as the calibration mode. Probes were injected at a volume of 20 μL into graphite wall tubes. The mean absorbances of duplicate injections were used throughout the study.

Binding Studies with a Selenopeptide. The substances were dissolved in 10% acetonitrile to a concentration of 5 mM and incubated at 37 °C for 48 h with a selenium-containing decamer AGUVGAGLIK at a molar ratio of complex-to-peptide of 5:1. The

peptide was previously treated at a 1:5 ratio with dithiothreitol for 1 h. ESI-MS and MS/MS spectra were recorded with a Finnigan LTQ XL mass spectrometer (Thermo Electron Corp., San Jose, CA), which was operated in the positive ion mode with a capillary temperature of 200 °C and a spray voltage of 1.8 kV. Direct injection of samples into the mass spectrometer was performed at a flow rate of 1.0 μL min^{-1}. The relative collision energy for collision-induced dissociation was set at 35%.

TrxR/GR Inhibition Assay. To determine the inhibition of TrxR and GR, an established microplate reader-based assay was performed with minor modifications.[10] For this purpose, commercially available rat liver TrxR and baker yeast GR (both from Sigma-Aldrich) were used and diluted with distilled water to achieve a concentration of 2.0 U/mL. The compounds were freshly dissolved as stock solutions in DMF. To each 25 μL aliquot of the enzyme solution, each 25 μL of potassium phosphate buffer, pH 7.0, containing the compounds in graded concentrations or vehicle (DMF) without compounds (control probe) was added, and the resulting solutions (final concentration of DMF: max. 0.5% v/v) were incubated with moderate shaking for 75 min at 37 °C in a 96-well plate. To each well, 225 μL of reaction mixture (1000 μL of reaction mixture consisted of 500 μL of potassium phosphate buffer, pH 7.0, 80 μL of 100 mM EDTA solution, pH 7.5, 20 μL of 0.05% BSA solution, 100 μL of 20 mM NADPH solution, and 300 μL of distilled water) was added, and the reaction was started by the addition of 25 μL of an 20 mM ethanolic DTNB solution. After proper mixing, the formation of 5-TNB was monitored with a microplate reader (Perkin-Elmer VictortmX4) at 405 nm in 10 s intervals for 6 min. The increase in 5-TNB concentration over time followed a linear trend ($r^2 \geq 0.99$), and the enzymatic activities were calculated as the slopes (increase in absorbance per second) thereof. For each tested compound, the noninterference with the assay components was confirmed by a negative control experiment using an enzyme free solution. The EC_{50} values were calculated as the concentration of compound decreasing the enzymatic activity of the untreated control by 50% and are given as the means and errors of 3–6 independent experiments.

GPx Inhibition Assay. To determine the inhibition of GPx, an established microplate reader-based assay was performed with minor modifications.[48,49] For this purpose, commercially available fetal bovine erythrocytes GPx (Sigma-Aldrich) were used and diluted with distilled water to achieve a concentration of 100 ng/mL. The compounds were freshly dissolved as stock solutions in DMF. To each 35 μL aliquot of the enzyme solution, each 35 μL of buffer, pH 7.0, containing the compounds in graded concentrations or vehicle (DMF) without compounds (control probe) was added, and the resulting solutions (final concentration of DMF: max. 0.5% v/v) were incubated with moderate shaking for 75 min at 37 °C in a 96-well plate. To each well, 25 μL of a 4 U/mL GR solution in water and 200 μL of reaction mixture (1000 μL of reaction mixture consisted of 600 μL of Hepes/TrisHCl 1:1 50 mM buffer, pH 7.0, 100 μL of 50 mM EDTA solution, pH 7.5, 100 μL of 50 mM reduced glutathione solution, 100 μL of 50 mM NADPH solution, and 100 μL of distilled water) were added, and the reaction was started by the addition of 25 μL of a 5 mM *t*-butylperoxide solution. After proper mixing, the reduction of NADPH was monitored with a microplate reader (Perkin-Elmer VictorX4) at 340 nm in 10 s intervals for 1 min. The decrease in NADPH concentration over time followed a linear trend ($r^2 \geq 0.99$), and the enzymatic activities were calculated as the slopes (decrease in absorbance per second) thereof. For each tested compound, the noninterference with the assay components was confirmed by a negative control experiment using a GPx/GR-enzyme free solution. The EC_{50} values were calculated as the concentration of compound decreasing the GPx activity of an untreated control by 50% and are given as the means and errors of three independent experiments.

Antiproliferative Effects in MCF-7, HT-29, and HEK-293 Cells. The antiproliferative effects in MCF-7, HT-29, and HEK-293 cells after 72 h (HT-29 and HEK-293) or 96 h (MCF-7) exposure to the gold complexes were evaluated according to a procedure already described in the literature.[50] For the experiments, the compounds were prepared freshly as stock solutions in DMF and diluted with the cell culture medium to the final assay concentrations (0.1% v/v DMF). The cells were cultured in a 75 cm^2 flask with 10 mL of cell culture medium. A volume of 100 μL of 10000 cells/mL medium (MCF-7 and HEK-293) or 4500 cells/mL (HT-29) was seeded in 96-well plates and incubated for 48 (HT-29) or 72 h (MCF-7 and HEK-293) at 37 °C under 5% CO_2. Afterward, the medium was removed and replaced with medium containing the substances in different concentrations. The cells were exposed to the complexes for 72 (HT-29) or 96 h (MCF-7 and HEK-293). The medium was removed, and the cells were washed with PBS and stained with 100 μL of 0.02% crystal violet for 30 min. The excess of crystal violet was removed, the plates were washed with water and dried, 180 μL of 70% ethanolic solution was added to each well, and the plates were read at 595 nm in a microplate reader (VictorX4, PerkinElmer) after 3–4 h of gentle shaking. The IC_{50} values were calculated as the concentrations reducing proliferation of untreated control cells by 50% and are given as the means and errors of two independent experiments (each performed with $n = 6$).

Phase Contrast Video Microscopic Imaging. MCF-7 cells were grown in phenol red-free medium [DMEM 4.5 g/L glucose, with L-glutamine, supplemented with 50 mg/L gentamycine and 10% (v/v) FCS] in a 22.1 cm^2 tissue culture dish until approximately 60% confluency. The medium was replaced with 4.0 mL of phenol red-free medium containing 5.0 μM **1**, 1.0 μM **2** or **3** (0.1% v/v DMF), or only the DMF vehicle as a control. The tissue culture dish was placed under a EVOSxl digital microscope, and pictures were subsequently taken in 5 min intervals for 14 h.

Uptake into Cells and Mitochondria. MCF-7 breast cancer cells were grown until at least 80% confluence in 75 (for cellular uptake) or 175 cm^2 (for uptake into mitochondria) cell culture flasks. Stock solutions of 3.0 mM of the gold complexes in DMF were freshly prepared and diluted with culture medium supplemented with 10% (v/v) FCS or with serum-free medium (final concentration of DMF: 0.1% v/v). The cell culture medium of the flasks was replaced with medium containing the substances and incubated for 0, 1, 2, 4, 6, and 12 h at 37 °C/5% CO_2. The intact cell pellets were collected after trypsinization (trypsin 0.05%) and centrifugation (3000*g*, 5 min). Cell pellets were lysed with a 1000 μL of Tris-HCl buffer (10 mM Tris-HCl, 10 mM NaCl, and 10 mM $MgCl_2$, pH 7.4) in a prechilled dounce homogenizator on ice. For cellular uptake studies, an aliquot of 20 μL was removed for protein quantification by Bradford method, and 100 μL of the lysate was treated with 10 μL of 1% Triton X100 and investigated by AAS (see above). Mitochondria and cytosol were isolated using the Thermo Scientific mitochondria isolation kit for cultured cells (batch number 89874) according to the manufacturer's instructions. The obtained fractions were dissolved in 1000 μL of water (for mitochondria), an aliquot of 20 μL was removed for protein quantification by the Bradford method, and 100 μL was taken, treated with 10 μL of 1% Triton X100 and investigated by AAS (see above). Results were expressed as nmol gold/mg protein as means and errors of two independent experiments.

Isolation of Mouse Liver Mitochondria. Mitochondria were isolated according to described procedures with minor modifications.[51,52] Mouse (wildtype, C57BL/6) liver mitochondria were isolated by Dounce homogenization and differential centrifugation. The entire isolation process took place in isolation buffer (300 mM trehalose, 10 mM HEPES-KOH, pH 7.7, 10 mM KCl, 1 mM EGTA, 1 mM EDTA, and 0.1% fatty acid-free BSA). The homogenate was centrifuged for 5 min at 1000*g* and 4 °C. The supernatant was collected and centrifuged for 2 min at 13000 rpm and 4 °C. The mitochondrial pellet was resuspended in a small volume of isolation buffer, and the last centrifugation step was repeated. After the final mitochondria pellet was resuspended in isolation buffer, the protein content was estimated by Bradford assay.

Measurement of Mitochondrial Oxygen Consumption. The measurement was performed using OxoPlate (PreSens, Germany) 96-well plates, which contain an immobilized oxygen sensor at the bottom of each well. Fluorescence was measured in dual mode, excitation 540 nm and emission 650 nm, with reference emission 590 nm. The signal ratio 650 nm/590 nm corresponds to the oxygen partial pressure. The

calibration of the fluorescence reader was performed using a two-point calibration with oxygen-free water (1% Na_2SO_3) and air-saturated water with an oxygen partial pressure corresponding to 0 and 100%, respectively. Eighteen micrograms of freshly isolated mitochondria was suspended in 100 μL of respiration buffer (25 mM sucrose, 100 mM KCl, 75 mM mannitol, 5 mM $MgCl_2$, 10 mM KH_2PO_4, 0.5 mM EDTA, 10 mM TRIS, and 0.1% fatty acid-free BSA, pH 7.4) containing 10 mM pyruvate, 2 mM malate, 2 mM ADP, and 0.5 mM ATP to activate oxidative phosphorylation. Fluorescence was measured continuously for 400 min with kinetic intervals of 5 min by a Tecan Safire^2 (Tecan, Maennedorf, Switzerland) microplate reader at 37 °C. During the measurements, the plates were sealed with a breathable membrane (Diversified Biotech, Boston, MA). Additional controls were 5 μM rotenone (Sigma-Aldrich) as an inhibitor of respiratory chain complex I and 1 μM CCCP (carbonyl cyanide 3-chlorophenylhydrazone, Sigma-Aldrich) as an uncoupling agent, capable of increasing electron flow through the respiratory chain thereby increasing the oxygen consumption. Experiments were repeated with comparable results. One experiment is depicted.

MMP ($\Delta\psi_m$). Jurkat cells were cultivated in RPMI (PAA) with 10% FCS (PAA) at 37 °C, 5% CO_2, and 95% humidity. A 2.5×10^5 amount of Jurkat cells was seeded in cell culture plates and treated with the indicated compounds for 0.5, 3, 6, and 8 h. Cells were then stained with 500 nM JC-1 (5,5,6,6-tetrachloro-1,1,3,3-tetraethylbenzimidazolylcarbocyanineiodide, Sigma-Aldrich) for 15 min at 37 °C, collected, and analyzed using a FACSCalibur (Beckton Dickinson) and CellQuest Pro analysis software (Beckton Dickinson). Excitation and emission settings were 488 nm, 515−545 nm (FL1 channel) for JC monomers, and 564−606 nm (FL2 channel) for JC aggregates. Experiments were repeated with comparable results. One experiment is depicted.

Annexin V/PI Staining. Jurkat cells were treated with the indicated concentration of the substance for 48 h, collected, and stained with Annexin V-FITC (eBioscience) according to the manufacturer's recommendation. Briefly, approximately 5.0×10^5 cells were resuspended in 50 μL of Annexin V staining buffer (10 mM HEPES, 140 mM NaCl, and 2.5 mM $CaCl_2$, pH 7.4), 2.5 μL of AnnexinV-conjugate and 1.25 μL of PI solution (1 mg/mL) were added, and the probes were incubated in the dark at room temperature for 15 min. The signal intensity was analyzed using a FACS Calibur (Becton Dickinson) and CellQuest Pro (BD) analysis software. Excitation and emission settings were 488 nm, 515−545 nm (FL1 channel) for Annexin V-FITC, and 564−606 nm (FL2 channel) for PI. Experiments were repeated with comparable results. One experiment is depicted.

ROS Formation. JURKAT cells were cultivated in standard conditions, and cells were incubated with the compounds for 24 h as indicated. After incubation, cells were collected, centrifuged at 0.2*g* (1500 rpm), and resuspended in FACS buffer (D-PBS, Gibco, + 1% BSA, PAA). Cell suspensions were treated with DHE (dihydroethidium, Sigma, 5 μL of 5 mM stock solution per 1.0 mL of cell suspension containing 10^6 cells) at room temperature in the dark for 15 min, washed one more time with FACS buffer, and immediately analyzed using a FACSCalibur (Becton Dickinson) and CellQuest Pro (BD) analysis software. Excitation and emission settings were 488 and 564−606 nm (FL2 filter), respectively. Important note: Although DHE is known to interact only with superoxide anion, the intensity of fluorescence is commonly considered as a reflection of total intracellular ROS. Experiments were repeated with comparable results. One experiment is depicted.

Effects on Cell Metabolism. Online measurement of cell metabolism and morphological changes was done using a Bionas 2500 biosensor chip system (Bionas, Rostock, Germany). The metabolic sensor chips (SC 1000) include ion-sensitive field-effect transistors to record pH changes, a Clark type electrode to monitor oxygen consumption, and interdigitated electrode structures to measure impedance under the cell layer. Approximately 1.5×10^5 (150000 cell/chip) of MCF-7 cells were seeded directly onto each sensor chip in 450 μL of DMEM (PAA, E15-883) with penicillin/streptomycin and 10% (v/v) FCS (PAA) and incubated at 37 °C, 5% CO_2, and 95% humidity for 24 h. The cell number used resulted in approximately 80−90% confluence of the cells on the chip surface after 24 h. This was the starting condition for online monitoring. Sensor chips with cells were then transferred to the Bionas 2500 analyzer in which medium is continuously exchanged in 8 min cycles (4 min exchange of medium and 4 min without flow), during which the parameters were measured. The running medium used during analysis was DMEM (PAN Biotech GmbH, Aidenbach, Germany) without carbonate buffer and only weakly buffered with 1 mM Hepes and reduced FCS (0.1%). For drug activity testing, included were the following steps: (1) 5 h equilibration with running medium (RM), (2) drug exposure with substances freshly dissolved in medium at indicated concentrations and indicated incubation time, (3) a drug-free step in which cells are again fed with running medium without substances, and (4) at the end of each experiment, the cell layers were removed by adding 0.2% Triton X-100 to obtain basic signal without living cells on the sensor surface as a negative control. Experiments were repeated with comparable results. One experiment is depicted.

■ ASSOCIATED CONTENT

Ⓢ Supporting Information

Molecular representation of the calculated geometries of gold(I) carbene complexes, a glutathione interaction study, more details of the MS/MS study of gold complexes incubated with a selenocysteine-containing peptide, additional data on the dose-dependent effects of gold(I) complexes on cancer cells, cytosolic uptake of gold complexes, cytochrome *c* release, and video microscopic imaging studies. This material is available free of charge via the Internet at http://pubs.acs.org.

■ AUTHOR INFORMATION

Corresponding Author

*Tel: +49 531 3912743. E-mail: ingo.ott@tu-bs.de.

■ ACKNOWLEDGMENTS

Financial support by Deutsche Forschungsgemeinschaft (DFG, Grant FOR-630) is gratefully acknowledged.

■ ABBREVIATIONS USED

BDE, bond dissociation energy; DLC, delocalized lipophilic cation; NHC, N-heterocyclic carbene; GPx, glutathione peroxidase; GR, glutathione reductase; TrxR, thioredoxin reductase; ROS, reactive oxygen species; MMP, mitochondrial membrane potential

■ REFERENCES

(1) Ott, I. On the medicinal chemistry of gold complexes as anticancer drugs. *Coord. Chem. Rev.* **2009**, *253*, 1670−1681.

(2) Berners-Price, S. J.; Filipovska, A. Gold compounds as therapeutic agents for human diseases. *Metallomics* **2011**, *3*, 863−873.

(3) Nobili, S.; Mini, E.; Landini, I.; Gabbiani, C.; Casini, A.; Messori, L. Gold Compounds as Anticancer Agents: Chemistry, Cellular Pharmacology, and Preclinical Studies. *Med. Res. Rev.* **2010**, *30*, 550−580.

(4) Che, C.-M.; Sun, R. W.-Y. Therapeutic applications of gold complexes: Lipophilic gold(III) cations and gold(I) complexes for anti-cancer treatment. *Chem. Commun.* **2011**, *47*, 9554−9560.

(5) Barnard, P. J.; Berners-Price, S. J. Targeting the mitochondrial cell death pathway with gold compounds. *Coord. Chem. Rev.* **2007**, *251*, 1889−1902.

(6) Zhang, X.; Frezza, M.; Milacic, V.; Ronconi, L.; Fan, Y.; Bi, C.; Fregona, D.; Dou, Q. P. Inhibition of Tumor Proteasome Activity by Gold−Dithiocarbamato Complexes via Both Redox-Dependent and -Independent Processes. *J. Cell. Biochem.* **2010**, *109*, 162−172.

(7) Marzano, C.; Ronconi, L.; Chiara, F.; Giron, M. C.; Faustinelli, I.; Cristofori, P.; Trevisan, A.; Fregona, D. Gold(III)-dithiocarbamato

anticancer agents: Activity, toxicology and histopathological studies in rodents. *Int. J. Cancer* **2011**, *129*, 487−496.
(8) Sun, R. W.-Y.; Che, C.-M. The anti-cancer properties of gold(III) compounds with dianionic porphyrin and tetradentate ligands. *Coord. Chem. Rev.* **2009**, *253*, 1682−1691.
(9) Hickey, J. L.; Ruhayel, R. A.; Barnard, P. J.; Baker, M. V.; Berners-Price, S. J.; Filipovska, A. Mitochondria-targeted chemotherapeutics: The rational design of gold(I) N-heterocyclic carbene complexes that are selectively toxic to cancer cells and target protein selenols in preference to thiols. *J. Am. Chem. Soc.* **2008**, *130*, 12570−12571.
(10) Rubbiani, R.; Kitanovic, I.; Alborzinia, H.; Can, S.; Kitanovic, A.; Onambele, L. A.; Stefanopoulou, M.; Geldmacher, Y.; Sheldrick, W. S.; Wolber, G.; Prokop, A.; Wölfl, S.; Ott, I. Benzimidazol-2-ylidene Gold(I) Complexes Are Thioredoxin Reductase Inhibitors with Multiple Antitumor Properties. *J. Med. Chem.* **2010**, *53*, 8608−8618.
(11) Siciliano, T. J.; Deblock, M. C.; Hindi, K. M.; Durmus, S.; Panzner, M. J.; Tessier, C. A.; Youngs, W. J. Synthesis and anticancer properties of gold(I) and silver(I) N-heterocyclic carbene complexes. *J. Organomet. Chem.* **2011**, *696*, 1066−1071.
(12) Bindoli, A.; Rigobello, M. P.; Scutari, G.; Gabbiani, C.; Casini, A.; Messori, L. Thioredoxin reductase: A target for gold compounds acting as potential anticancer drugs. *Coord. Chem. Rev.* **2009**, *253*, 1692−1707.
(13) Krishnamurthy, D.; Karver, M. R.; Fiorillo, E.; Orru, V.; Stanford, S. M.; Bottini, N.; Barrios, A. M. Gold(I)-mediated inhibition of protein tyrosine phosphatases: a detailed in vitro and cellular study. *J. Med. Chem.* **2008**, *51*, 4790−4795.
(14) Karver, M. R.; Krishnamurthy, D.; Kulkarni, R. A.; Bottini, N.; Barrios, A. M. Identifying Potent, Selective Protein Tyrosine Phosphatase Inhibitors from a Library of Au(I) Complexes. *J. Med. Chem.* **2009**, *52*, 6912−6918.
(15) Mendes, F.; Groessl, M.; Nazarov, A. A.; Tsybin, Y. O.; Sava, G.; Santos, I.; Dyson, P. J.; Casini, A. Metal-Based Inhibition of Poly(ADP-ribose) Polymerase - The Guardian Angel of DNA. *J. Med. Chem.* **2011**, *54*, 2196−2206.
(16) Rigobello, M. P.; Scutari, G.; Folda, A.; Bindoli, A. Mitochondrial thioredoxin reductase inhibition by gold(I) compounds and concurrent stimulation of permeability transition and release of cytochrome c. *Biochem. Pharmacol.* **2004**, *67*, 689−696.
(17) Holmgren, A.; Lu, J. Thioredoxin and thioredoxin reductase: Current research with special reference to human disease. *Biochem. Biophys. Res. Commun.* **2010**, *396*, 120−124.
(18) Pratesi, A.; Gabbiani, C.; Ginanneschi, M.; Messori, L. Reactions of medicinally relevant gold compounds with the C-terminal motif of thioredoxin reductase elucidated by MS analysis. *Chem. Commun.* **2010**, *46*, 7001−7003.
(19) Gabbiani, C.; Mastrobuoni, G.; Sorrentino, F.; Dani, B.; Rigobello, M. P.; Bindoli, A.; Cinellu, M. A.; Pieraccini, G.; Messoria, L.; Casini, A. Thioredoxin reductase, an emerging target for anticancer metallodrugs. Enzyme inhibition by cytotoxic gold(III) compounds studied with combined mass spectrometry and biochemical assays. *Med. Chem. Commun.* **2011**, *2*, 50−54.
(20) Shaw, C. F. Gold-based therapeutic agents. *Chem. Rev.* **1999**, *99*, 2589−2600.
(21) John, A.; Gosh, P. Fascinating frontiers of N/O-functionalized N-heterocyclic carbene chemistry: From chemical catalysis to biomedical applications. *Dalton Trans.* **2010**, *39*, 7183−7206.
(22) Bourissou, D.; Guerret, O.; Gabbai, F. P.; Bertrand, G. Stable Carbenes. *Chem. Rev.* **2000**, *100*, 39−91.
(23) Gasser, G.; Ott, I.; Metzler-Nolte, N. Organometallic Anticancer Compounds. *J. Med. Chem.* **2011**, *54*, 3−25.
(24) Teyssot, M.-L.; Jarrousse, A.-S.; Manin, M.; Chevry, A.; Roche, S.; Norre, F.; Beaudoin, C.; Morel, L.; Boyer, D.; Mahiou, R.; Gautier, A. Metal-NHC complexes: a survey of anti-cancer properties. *Dalton Trans.* **2009**, 6894−6902.
(25) Ricca, A.; Bauschlicher, C. W. Successive H2O Binding Energies for Fe(H2O)n+. *J. Phys. Chem.* **1995**, *99*, 9003−9007.
(26) Hrusak, J.; Hertwig, R.; Schroeder, D.; Schwerdtfeger, P.; Koch, W.; Schwarz, H. Relativistic Effects in Cationic Gold(I) Complexes: A Comparative Study of ab Initio Pseudopotential and Density Functional Methods. *Organometallics* **1995**, *14*, 1284−1291.
(27) Boys, S. F.; Bernardi, F. Calculation of Small Molecular Interactions by Differences of Separate Total Energies—Some Procedures with Reduced Errors. *Mol. Phys.* **1970**, *19*, 553.
(28) Snyder, R. M.; Mirabelli, C. K.; Crooke, S. T. Cellular association, intracellular distribution, and efflux of auranofin via sequential ligand exchange reactions. *Biochem. Pharmacol.* **1986**, *35*, 923−932.
(29) Iqbal, M. S.; Taqi, S. G.; Arif, M.; Wasim, M.; Sher, M. In Vitro Distribution of Gold in Serum Proteins after Incubation of Sodium Aurothiomalate and Auranofin with Human Blood and its Pharmacological Significance. *Biol. Trace Elem. Res.* **2009**, *130*, 204−209.
(30) Ott, I.; Qian, X.; Xu, Y.; Vlecken, D. H. W.; Marques, I. J.; Kubutat, D.; Will, J.; Sheldrick, W. S.; Jesse, P.; Prokop, A.; Bagowski, C. P. A Gold(I) Phosphine Complex Containing a Naphthalimide Ligand Functions as a TrxR Inhibiting Antiproliferative Agent and Angiogenesis Inhibitor. *J. Med. Chem.* **2009**, *52*, 763−770.
(31) Ott, I.; Kircher, B.; Bagowski, C. P.; Vlecken, D. H. W.; Ott, E. B.; Will, J.; Bensdorf, K.; Sheldrick, W. S.; Gust, R. Modulation of the biological properties of aspirin by formation of a bioorganometallic derivative. *Angew. Chem., Int. Ed.* **2009**, *48*, 1160−1163.
(32) Ralph, S. J.; Neuzil, J. Mitochondria as targets for cancer therapy. *Mol. Nutr. Food Res.* **2009**, *53*, 9−28.
(33) Sundelacruz, S.; Levin, M.; Kaplan, D. L. Role of Membrane Potential in the Regulation of Cell Proliferation and Differentiation. *Stem Cell Rev. Rep.* **2009**, *5*, 231−246.
(34) Heerdt, B. G.; Houston, M. A.; Augenlicht, L. H. The Intrinsic Mitochondrial Membrane Potential of Colonic Carcinoma Cells Is Linked to the Probability of Tumor Progression. *Cancer Res.* **2005**, *65*, 9861−9867.
(35) Chauhan, D.; Pandey, P.; Ogata, A.; Teoh, G.; Krett, N.; Halgren, R.; Rosen, S.; Kufe, D.; Kharbanda, S.; Anderson, K. Cytochrome c-dependent and -independent Induction of Apoptosis in Multiple Myeloma Cells. *J. Biol. Chem.* **1997**, *272*, 29995−29997.
(36) Alborzinia, H.; Can, S.; Holenya, P.; Scholl, C.; Lederer, E.; Kitanovic, I.; Wölfl, S. Real-time monitoring of Cisplatin-induced cell death. *Plos One* **2011**, *6*, e19714.
(37) Modica-Napolitano, J. S.; Aprille, J. R. Delocalized lipophilic cations selectively target the mitochondria of carcinoma cells. *Adv. Drug Delivery Rev.* **2001**, *69*, 63−70.
(38) Jellicoe, M. M.; Nichols, S. J.; Callus, B. A.; Baker, M. V.; Barnard, P. J.; Berners-Price, S. J.; Whelan, J.; Yeoh, G. C.; Filipovska, A. Bioenergetic differences selectively sensitize tumorigenic liver progenitor cells to a new gold(I) compound. *Carcinogenesis* **2008**, *29*, 1124−1133.
(39) Baker, M.; Barnard, P. J.; Berners-Price, S. J.; Brayshaw, S. K.; Hickey, J. L.; Skelton, B. W.; White, A. H. Cationic, linear Au(I) N-heterocyclic carbene complexes: synthesis, structure and anti-mitochondrial activity. *Dalton Trans.* **2006**, 3708−3715.
(40) Baker, M. V.; Barnard, P. J.; Berners-Price, S. J.; Brayshaw, S. K.; Hickey, J. L.; Skelton, B. W.; White, A. H. Synthesis and structural characterisation of linear Au(I) N-heterocyclic carbene complexes: New analogues of the Au(I) phosphine drug Auranofin. *J. Organomet. Chem.* **2005**, *690*, 5625−5635.
(41) Frisch, M. J.; Trucks, G. W.; Schlegel, H. B.; Scuseria, G. E.; Robb, M. A.; Cheeseman, J. R.; Scalmani, G.; Barone, V.; Mennucci, B.; Petersson, G. A.; Nakatsuji, H.; Caricato, M.; Li, X.; Hratchian, H. P.; Izmaylov, A. F.; Bloino, J.; Zheng, G.; Sonnenberg, J. L.; Hada, M.; Ehara, M.; Toyota, K.; Fukuda, R.; Hasegawa, J.; Ishida, M.; Nakajima, T.; Honda, Y.; Kitao, O.; Nakai, H.; Vreven, T.; Montgomery, J. A., Jr.; Peralta, J. E.; Ogliaro, F.; Bearpark, M.; Heyd, J. J.; Brothers, E.; Kudin, K. N.; Staroverov, V. N.; Kobayashi, R.; Normand, J.; Raghavachari, K.; Rendell, A.; Burant, J. C.; Iyengar, S. S.; Tomasi, J.; Cossi, M.; Rega, N.; Millam, J. M.; Klene, M.; Knox, J. E.; Cross, J. B.; Bakken, V.; Adamo, C.; Jaramillo, J.; Gomperts, R.; Stratmann, R. E.; Yazyev, O.; Austin, A. J.; Cammi, R.; Pomelli, C.; Ochterski, J. W.; Martin, R. L.; Morokuma, K.; Zakrzewski, V. G.; Voth, G. A.; Salvador, P.;

Dannenberg, J. J.; Dapprich, S.; Daniels, A. D.; Farkas, O.; Foresman, J. B.; Ortiz, J. V.; Cioslowski, J.; Fox, D. J. *Gaussian 09*; Gaussian, Inc.: Wallingford, CT, 2009.
(42) Feller, D. The role of databases in support of computational chemistry calculations. *J. Comput. Chem.* **1996**, *17*, 1571−1586.
(43) Schuchardt, K. L.; Didier, B. T.; Elsethagen, T.; Sun, L. S.; Gurumoorthi, V.; Chase, J.; Li, J.; Windus, T. L. Basis set exchange: A community database for computational sciences. *J. Chem. Inf. Model.* **2007**, *47*, 1045−1052.
(44) Barone, V.; Cossi, M.; Tomasi, J. Geometry optimization of molecular structures in solution by the polarizable continuum model. *J. Comput. Chem.* **1998**, *19*, 404−417.
(45) Miertus, S.; Tomasi, J. Approximate Evaluations of the Electrostatic Free-Energy and Internal Energy Changes in Solution Processes. *Chem. Phys.* **1982**, *65*, 239−245.
(46) Tomasi, J.; Mennucci, B.; Cammi, R. Quantum mechanical continuum solvation models. *Chem. Rev.* **2005**, *105*, 2999−3093.
(47) Ott, I.; Scheffler, H.; Gust, R. Development of a Method for the Quantification of the Molar Gold Concentration in Tumour Cells Exposed to Gold-Containing Drugs. *ChemMedChem* **2007**, *2*, 702−707.
(48) Little, C.; Olinescu, R.; Reid, I. G.; O'Brien, P. J. Properties and Regulation of Glutathione Peroxidase. *J. Biol. Chem.* **1970**, *245*, 3632−3636.
(49) Gandin, V.; Fernandes, A. P.; Rigobello, M. P.; Dani, B.; Sorrentino, F.; Tisato, F.; Björnstedt, M.; Bindoli, A.; Sturaro, A.; Rella, R.; Marzano, C. Cancer Cell Death Induced by Phosphine Gold(I) Compounds Targeting Thioredoxin Reductase. *Biochem. Pharmacol.* **2010**, *79*, 90−101.
(50) Scheffler, H.; You, Y.; Ott, I. Comparative studies on the cytotoxicity, cellular and nuclear uptake of a series of chloro gold(I) phosphine complexes. *Polyhedron* **2010**, *29*, 66−69.
(51) Yamaguchi, R.; Andreyev, A.; Murphy, A. N.; Perkins, G. A.; Ellisman, M. H.; Newmeyer, D. D. Mitochondria frozen with trehalose retain a number of biological functions and preserve outer membrane integrity. *Cell Death Differ.* **2007**, *14*, 616−624.
(52) Fernández-Vizarra, E.; López-Pérez, M. J.; Enriquez, J. A. Isolation of biogenetically competent mitochondria from mammalian tissues and cultured cells. *Methods* **2002**, *26*, 292−297.